Supplementary Information
Suppression of AMOC variability at increased CO_2

Douglas G. MacMartin, Laure Zanna and Eli Tziperman

February 26, 2016

1 Supplemental figures

Several additional figures provide some useful details. Figure S1 shows the time response of AMOC at 26, 45, and 60°N from the preindustrial simulation, similar to Fig. 1 in the main text for the $4\times CO_2$ simulation; the oscillatory behavior at the lower latitudes is apparent. Figure S2 shows the time-response for a simulation where CO_2 is increased gradually at 1% per year rather than abruptly as in the $4\times CO_2$ simulation to evaluate whether the observed changes depend on the unrealistic abrupt nature of the forcing; there is no corresponding quasi-equilibrium state in this simulation. Fig. S3 shows the evolution of upper ocean heat content anomalies before and after an AMOC minimum for the preindustrial simulation, similar to Figure 6 in the paper. Figure S4 is similar to Figure 4 in the main text, except that where Figure 4 evaluated relationships relative to AMOC at 45°N for the preindustrial and 60°N for the $4\times CO_2$ simulations, Fig. S4 evaluates the relationships in both simulations for AMOC at 45°N. While this is less useful for understanding whether the "new" oscillation at 60° in the $4\times CO_2$ simulation arises from a similar mechanism as the lower-latitude oscillation in the preindustrial case, it is useful for illustrating that the differences apparent in Figure 4 are not simply a result of having evaluating relationships at a different latitude. Finally, the effect of AMOC variability on sea ice in the $4\times CO_2$ simulation is shown in Fig. S5.

2 Brief review of transfer functions

The following text is based closely on MacMynowski and Tziperman (2010). The frequency-dependent "transfer function" (e.g., Astrom and Murray, 2008) estimates the linear causal relationship between any pair of variables. Thus, the relationship between an "input variable" (X) and an "output variable" (Y) can be written as $Y = T_{XY}X$, with T_{XY} the transfer function. It is convenient to first derive the (complex) transfer function directly from an example of a differential equation describing the dynamics, although as we will see below the knowledge of the governing equation is not required. For example, consider the following equation,

$$\dot{Y} = \mu X - \epsilon Y. \tag{S1}$$

By taking the Fourier transform with a frequency f, we have

$$2\pi i f \hat{Y}(f) = \mu \hat{X}(f) - \epsilon \hat{Y}(f). \tag{S2}$$

The transfer function is now defined by

$$T_{XY}(s) \equiv \frac{\hat{Y}(s)}{\hat{X}(s)} = \frac{\hat{Y}(s)\hat{X}^*(s)}{\hat{X}(s)\hat{X}^*(s)} = \mu \frac{1}{s+\epsilon}, \tag{S3}$$

where $s = 2\pi i f$ and $\hat{Y}(s)\hat{X}^*(s)$ is the cross correlation between the input X and output variable Y. As this demonstrates, the transfer function depends on frequency according to the differential operator in the relation between the input and output.

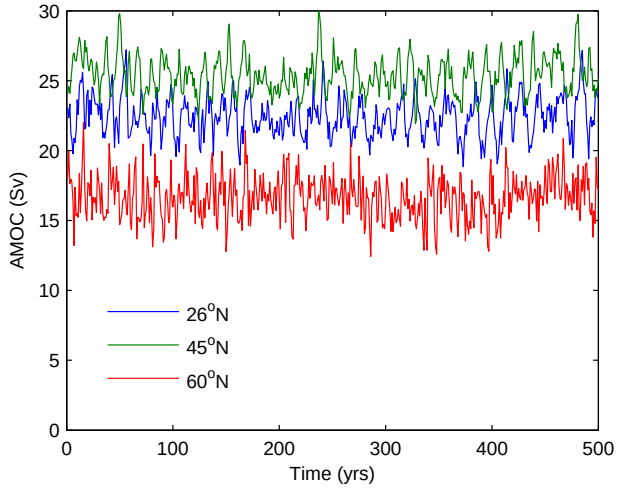

Figure S1: AMOC strength at 26, 45, and 60°N in the preindustrial or $1\times CO_2$ simulation.

However, a key advantage of the approach considered here is that the equation describing the relation between the input and output does not need to be known a priori, and indeed can be extracted from time series of the two. Given input and output time series $X(t)$ and $Y(t)$ and their Fourier transforms $\hat{X}(f)$ and $\hat{Y}(f)$, the transfer function between them may be obtained as the ratio of the cross-correlation to the auto-correlation in frequency space, as motivated by (S3) (e.g., Section 6.2, Swanson, 2000),

$$T_{XY}(f) = \frac{\left\langle \hat{X}(f)\hat{Y}^*(f) \right\rangle}{\left\langle \hat{X}(f)\hat{X}^*(f) \right\rangle} = \frac{S_{XY}(f)}{S_{XX}(f)}, \tag{S4}$$

where $S_{XY}(f)$ is calculated by dividing the time series into n segments and averaging the respective Fourier transforms. This averaging eliminates contributions that are not related to the input X,

$$S_{XY}(f) = \frac{1}{n}\sum_{k=1}^{n} \hat{X}_k(f)\hat{Y}_k^*(f). \tag{S5}$$

Error estimates of the transfer function are calculated from the coherence (eq. 6.2.21, Swanson, 2000).

At any frequency, the transfer function is simply a complex number, with both the magnitude and phase providing useful information about the relationship between the input and output variables.

References

Astrom, K. J. and Murray, R. M. (2008). *Feedback Systems: An Introduction for Scientists and Engineers.* Princeton University Press.

MacMynowski, D. G. and Tziperman, E. (2010). Testing and improving ENSO models by process using transfer functions. *Geophys. Res. Lett.*, 37:L19701, doi:10.1029/2010GL044050.

Swanson, D. C. (2000). *Signal processing for intelligent sensor systems.* CRC Press.

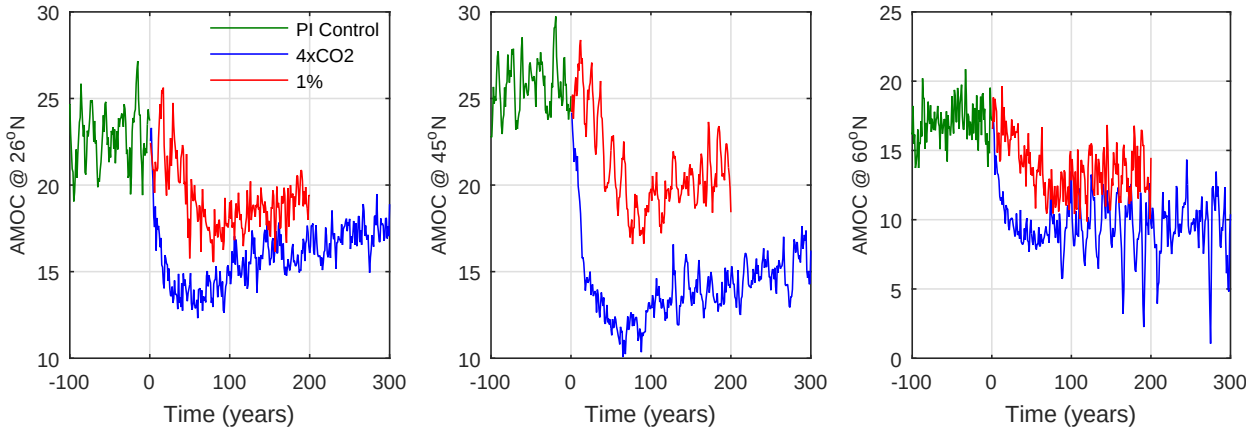

Figure S2: AMOC strength at 26, 45, and 60°N comparing abrupt $4\times CO_2$ simulation to 1% per year increase in CO_2 (red lines); the final 100 years of the preindustrial ($1\times CO_2$) simulation is shown for comparison. While the 1% simulation is not in steady-state over this time-interval, the suppression of variability at 26°N is evident; the effect at 45° is less clear.

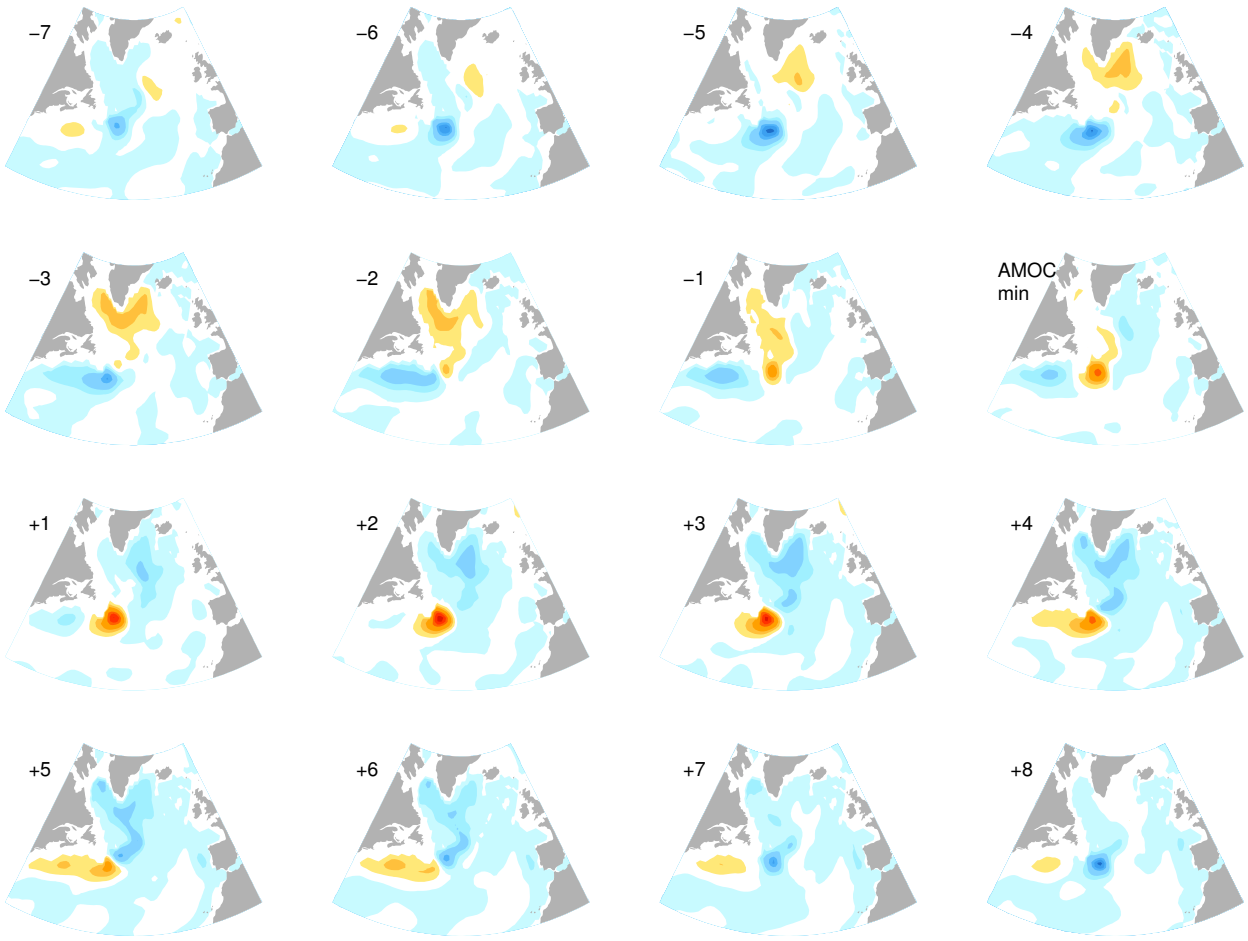

Figure S3: Evolution of upper ocean heat content anomaly, preindustrial ($1\times CO_2$) simulation. Panel labeled "AMOC min" shows the heat content averaged over AMOC minima (similar to Fig. 2(c)), remaining panels show the evolution prior to and after the minimum on the same color scale. Panels "-7" and "+8" are similar to the heat content averaged over AMOC maxima.

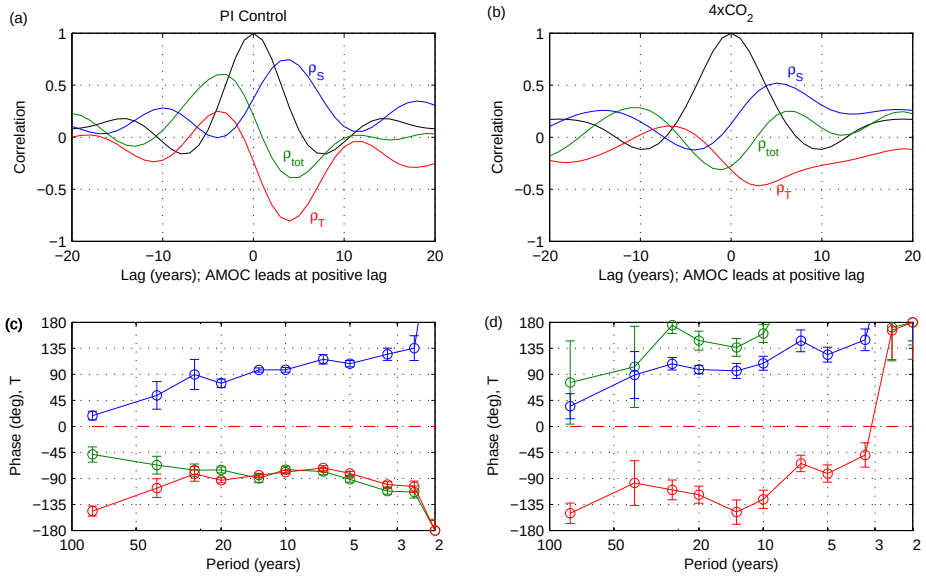

Figure S4: Temperature-salinity phase relations characterizing AMOC variability, with AMOC evaluated at 45°N in both preindustrial (left column) and $4\times CO_2$ (right column) simulations; panels (a) and (c) are identical to Figure 4. Upper row: lag-correlation plot (AMOC leads at positive lag) relating AMOC to itself (black line), to high-latitude density (green, ρ_{tot}), density due to temperature perturbations (red, ρ_T), and density due to salinity perturbations (blue, ρ_S); all variables are filtered at a 5-year period to focus on decadal variability. Temperature and salinity are averaged over the sinking region of 45-65°N and upper 1000 m in both cases.

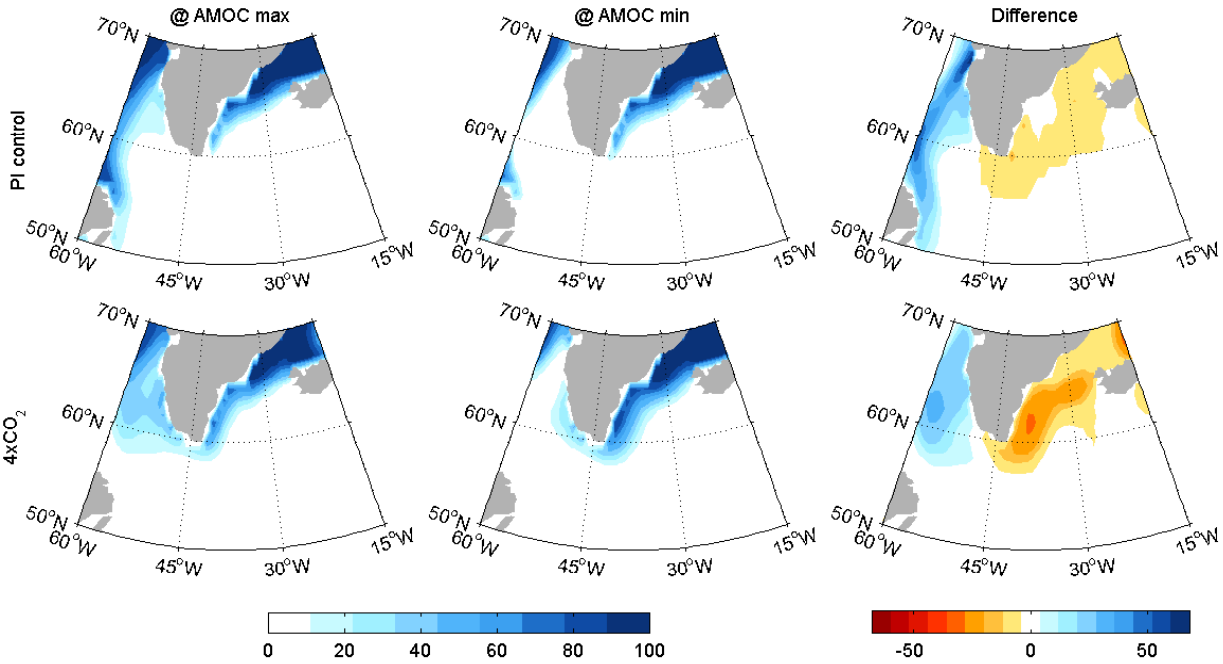

Figure S5: Sea ice concentration averaged over AMOC maxima (left), AMOC minima (middle) and the difference (right) for preindustrial (top) and $4\times CO_2$ simulations (bottom row). Compare with upper ocean heat content in Fig. 3(c,f); here the sea ice responds to the pattern of temperature variation. While AMOC variability in $4\times CO_2$ has less effect on mid-latitude variables than the AMOC variability in the preindustrial case, it can nonetheless be climatically important at high latitudes.